Low-lying structure of ^{15}C : information on the N=8 shell gap

J. Lois-Fuentes[1,*], B. Fernández-Domínguez[1], X. Pereira-López[1,2,3], F. Delaunay[2], W.N. Catford[4], A. Matta[2,4], N.A. Orr[2], T. Duguet[5,6], T. Otsuka[7], V. Somà[5], O. Sorlin[8], T. Suzuki[9,10], N.L. Achouri[2], M. Assié[11], S. Bailey[12], B. Bastin[8], Y. Blumenfeld[11], R. Borcea[15], M. Caamaño[1], L. Caceres[8], E. Clément[8], A. Corsi[5], N. Curtis[12], Q. Deshayes[2], F. Farget[8], M. Fisichella[13], G. de France[8], S. Franchoo[11], M. Freer[12], J. Gibelin[2], A. Gillibert[5], G.F. Grinyer[14], F. Hammache[11], O. Kamalou[8], A. Knapton[4], Tz. Kokalova[12], V. Lapoux[5], B. Le Crom[11], S. Leblond[2], F.M. Marqués[2], P. Morfouace[11], J. Pancin[8], L. Perrot[11], J. Piot[8], E. Pollacco[5], D. Ramos[1], D. Regueira-Castro[1], C. Rodríguez-Tajes[1,8], T. Roger[8], F. Rotaru[15], M. Sénoville[2], N. de Séréville[11], R. Smith[12,13], M. Stanoiu[15], I. Stefan[11], C. Stodel[8], D. Suzuki[11], J.C. Thomas[8], N. Timofeyuk[4], M. Vandebrouck[5,8], J. Walshe[12], and C. Wheldon[12]

[1]IGFAE and Dpt. de Física de Partículas, Univ. of Santiago de Compostela, E-15758, Santiago de Compostela, Spain.
[2]Université de Caen Normandie, ENSICAEN, CNRS/IN2P3, LPC Caen UMR6534, F-14000 Caen, France
[3]Center for Exotic Nuclear Studies, Institute for Basic Science (IBS), Daejeon 34126, Republic of Korea
[4]Department of Physics, University of Surrey, Guildford GU2 5XH, UK
[5]IRFU, CEA, Université Paris-Saclay, F-91191 Gif-sur-Yvette, France
[6]KU Leuven, Instituut voor Kern- en Stralingsfysica, 3001 Leuven, Belgium
[7]CNS, University of Tokyo, 7-3-1 Hongo, Bunkyo-ku, Tokyo, Japan
[8]GANIL, CEA/DRF-CNRS/IN2P3, Bd. Henri Becquerel, BP 55027, F-14076 Caen, France
[9]Department of Physics, College of Humanities and Sciences, Nihon University, Sakurajosui 3-25-40, Setagaya-ku, Tokyo, Japan
[10]NAT Research Center, NAT Corporation, 3129-45 Hirahara, Muramatsu, Tokai, Naka, 319-1112, Ibaraki, Japan
[11]Université Paris-Saclay, CNRS/IN2P3, IJCLab, 91405 Orsay, France
[12]School of Physics and Astronomy, University of Birmingham, Birmingham B15 2TT, UK
[13]INFN, Laboratori Nazionali del Sud, Via S. Sofia 44, Catania, Italy
[14]Department of Physics, University of Regina, Regina, SK S4S 0A2, Canada
[15]IFIN-HH, P. O. Box MG-6, 76900 Bucharest-Magurele, Romania

Abstract. The low-lying structure of ^{15}C has been investigated via the neutron-removal d(^{16}C, t) reaction. The experiment was performed at GANIL using a secondary ^{16}C beam produced by fragmentation in the LISE spectrometer at 17.2 MeV/nucleon with an intensity of 5×10^4 pps and 100% purity. The angle and energy of the light ejectile were detected by three MUST2 telescopes. The missing mass technique was used to reconstruct the excitation energy of ^{15}C. In this spectrum, two bound states were observed (gs and the first excited state) and two unbound resonant states above the neutron separation threshold (S_n = 1.218 MeV). From the differential cross sections, information on the angular momentum of the transferred nucleon and spectroscopic factors were deduced.
The excitation energies and the deduced spectroscopic factors of the negative parity states placed above the neutron separation energy are an important measurement of the 2p-1h configurations in ^{15}C. Our results show good agreement with shell-model calculations with the YSOX interaction and show a sensitivity to the N=8 shell gap.

1 Introduction

The study of the evolution of the shell structure when one moves away from the valley of stability has been one of the main tools used in the recent years to learn about fundamental properties of the nuclear interaction.

Nuclei far from the stability with large values of isospin, like the neutron-rich carbon isotopes, are useful to test the theoretical models and interactions. In particular, the shell model calculations with phenomenological interactions in the p-sd shell space (SFO tls [1, 2] and YSOX [3]) manage to reproduce energies and spectroscopic factors in the neutron-rich C isotopes. Still, there is a lack of neutron p-hole states data in this region, which give crucial constraints on the cross-shell part of the interactions. They may be tested by investigating the neutron configurations of the ^{15}C isotope, like the $(p)^{-1}(sd)^2$ which can be studied using the experimental data of cross-shell states measured via the ^{16}C(d,t) reaction.

Here we present the first study on the negative parity states in ^{15}C produced by a single-neutron pick-up reaction, ^{16}C(d,t)^{15}C. ^{16}C can be understood as a ^{14}C core coupled to two neutrons in the sd orbits, therefore the observed bound states in ^{15}C come from the removal of any

*e-mail: juan.lois.fuentes@usc.es

of these two neutrons. In addition a neutron could be also picked from the internal orbits from the core, producing characteristic p-hole states in the unbound part of the spectrum.

Several experiments have been performed in the past to study the structure of ^{15}C. Different probes were used, such us (d,p) [4], (t,p) [5], ^{13}C(^{18}O,^{16}O)^{15}C [6], breakup [7], and knockout experiments [8], but most of them focused on the positive parity states due to the low probability to produce p-hole states with their respective probes.

2 Experimental details

The experiment was performed at the LISE spectrometer in GANIL. It delivered a 17.2 *A* MeV ^{16}C beam produced by fragmentation with an intensity of 5×10^4 pps into a 1.37 mg/cm^2 CD_2 target. The beam direction was determined by a pair of multiwire proportional chambers, the Z of the beam-like particle was identified with a CHARISSA telescope [9] and the outgoing tritium was detected in 3 MUST2 [10] telescopes which covered the forward laboratory angles of the reaction ($10^o - 40^o$). Due to the low energy of the tritons produced in the reaction, only the first layer of MUST2 was used (300 μm of Si). Identification of the mass of the outgoing particle was performed with the E-ToF technique, using the energy deposit from the stopped particle in the Si and the time between the first beam tracking detector and MUST2. The first layer of MUST2 is a X-Y position sensitive DSSSD with a high granularity (strip step 0.8 mm) allowing hit position measurement and track reconstruction (and incident angle on target) of the incident beam trajectory with the upstream beam detector.

3 Data analysis

The kinetic energy of a particle depends both on its velocity and mass, following equation 1. Therefore, when one plots the residual energy vs ToF different lines appear according to the masses of the particles that reach MUST2. The left panel of figure 1 shows the identification matrix were A = 1, 2, 3, 4 and 16 are observed. Using the beam tracking detectors we can determine the hit position on the target and combining this information with the hit position in MUST2 we can determine the total flight length, which allows us to calculate the mass in an absolute way.

$$E \propto A \times \left(\frac{L}{ToF}\right)^2 \quad (1)$$

The experimental limitations due to the energy resolution and energy straggling in the target produces that the selection of the A = 3 cannot be performed directly with a simple gate on figure 1 or a sharp cut on the 1D mass plot shown in the central panel of the same figure. The right panel of figure 1 shows the evolution of the calculated mass with respect to the E_x (assuming ^{15}C), and it can be observed that at low E_x (which corresponds to low energy also in the left panel of figure 1) the lines are much closer. Then, the contamination of A=4 in the selection gate must be taken into account. In order to gate on A=3, $2\sigma_{A=3}$ and $1\sigma_{A=3}$ as lower and upper limits were imposed in order to minimize the main source of contamination, the penetration of α particles (A=4) in our selection cut. The selection was performed taking into account the evolution of A = 3 with the E_x.

Finally a gate was applied on A=2 and 4 in coincidence with the a Z=6 selection of the beam-like particle (which reduces significantly the α contamination). The result was scaled taking into account the percentage of each mass that sinks into the A=3 gate, being this a way of estimating the contamination in the final E_x spectrum.

The ToF vs E technique just selects the events in mass so the gate could be taking tritons or/and ^{3}He particles but different observations confirm the presence of only the first of them. First of all the Q-value of the ^{16}C(d,^{3}He)^{15}B reaction places its ground state at higher energy than any of states shown in this study, naturally separating both reactions. Moreover CHARISSA is used to gate on Z=6, which vetoes ^{15}B. In addition a detail look at the left panel of figure 1 shows that the line corresponding to A=3 abruptly ends around 9 MeV, the punchthrough of the ^{3}H, which confirms the absence of ^{3}He since it would extend up to 20 MeV.

The evolution of the resolution with the E_x was determined using the nptool simulations package [11], which includes the effects of the straggling of the particles in the target and the different layers from MUST2, the resolution of the detectors and the beam energy spread as well as the beam spot and the geometry of the set up. The simulation yields a resolution which decreases with E_x following a polynomial function where σ = 0.90 MeV is the value obtained for the ground state and 0.55 MeV for the state at 3 MeV. This fast evolution is produced by the smaller straggling of the tritons produced by states at higher energy.

3.1 Results

After the ^{3}H were selected with the A=3 gate described above, in coincidence with Z=6 for the beam-like particle, the E_x spectrum was built using the missing-mass technique. The spectrum displayed on figure 2 shows the E_x in the center of mass angular range 3º-15º and the fit to the present states. The limitations in energy resolution are responsible for the imperfect separation between the well established ground state and first excited state (0.74 MeV) which energies and spin-parity values are well known. The final fit was performed taking into account the evolution of the E_x resolution obtained using comparison to nptool simulations, fitting the two resonances with a Breit-Wigner convoluted with the experimental resolution. In addition the contribution of the background and the one-neutron (1n) phase space are also considered. The first resonance was already observed in previous experiments and J^π=1/2$^-$ was assigned, finding a natural width of ∼

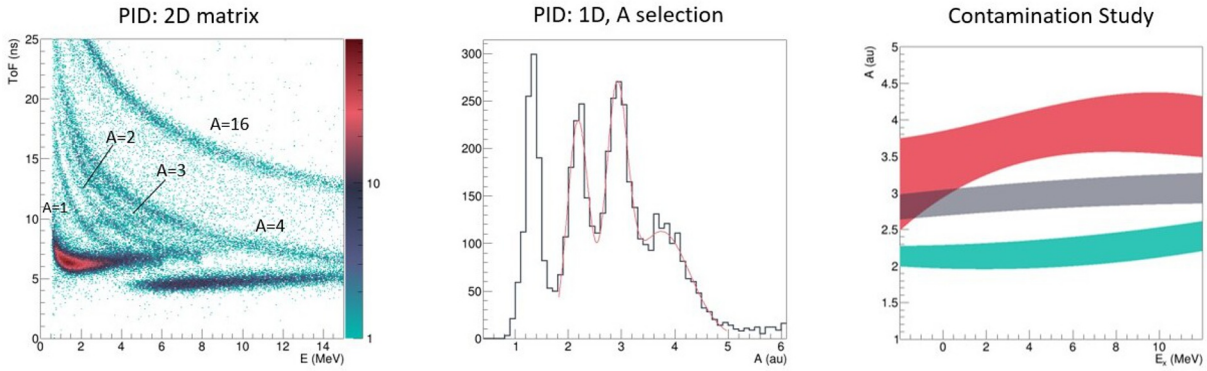

Figure 1. Particle identification plots. The left panel shows the ToF vs the residual energy in the silicon where we can clearly identify the different lines associated to each of the masses that arrive in MUST2. The central plot shows the 1D particle identification showing 4 peaks associated to the light particles. In order to built this plot the E and ToF from the left panel, and the flight length from the target to the hit position in MUST2 were used. The right panel shows evolution of each mass with respect to the E_x of ^{15}C, plotted with its 1σ bands which also evolves with E_x. Studying this plot we can obtain the contamination from A=2 and 4 into our A=3 gate.

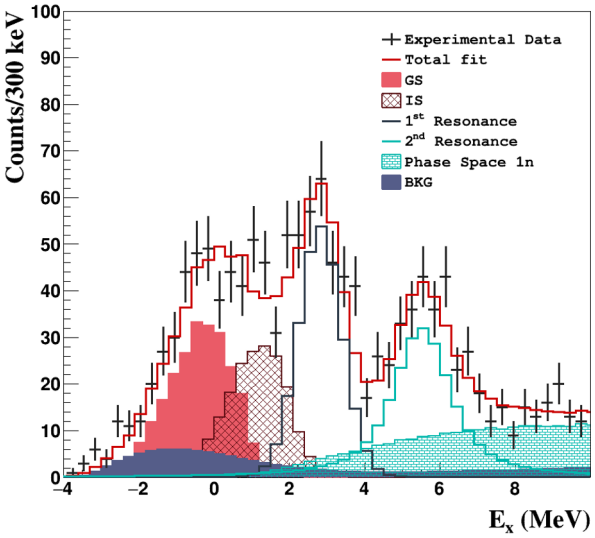

Figure 2. E_x spectrum fitted to the different states observed. In the case of the unbound states a Breit-Wigner fuction convoluted with the experimental resolution is used. The histogram in purple color corresponds to the different sources of background such as the contamination of A=2 and 4 in our A=3 gate. Finally in light blue we also consider the presence of the non-resonant continuum with the 1n phase space.

50 keV. There are works that point out the presence of different states in the region of our second unbound state, but we cannot firmly assign it to any of them. The result from the fitting procedure shows that in addition to the statistical uncertainties there is an overall systematic error in the excitation energy of ±0.35 MeV, which is deduced from the difference of the fit results with respect to the known E_x values of the ground state, first excited state, and first resonance. This error has different origins such as non linearities in the measurement of the energy that could not be properly addressed due to the limited statistics, preventing us from performing an ad-hoc calibration of the states. This systematic error does not have a large impact on our results since our main output from this analysis is the spectroscopic factor of the resonances, which relies on the yield distribution[1] .

Figure 3 presents the angular distributions which were obtained from the individual fits of the spectrum in $\Delta\theta_{CM}$ = 2° slices. They are plotted together with the finite-range Distorted-Wave Born Approximation (DWBA) calculations which are normalized to the data to extract the spectroscopic factors. The DWBA calculations were performed using for the input channel the parameterization of Haixia et al. [12], which was modified to reproduce elastic scattering also measured in the experiment [13, 14]. For the exit channel the optical model potential from Pang et al. [15] was applied. The <d|t> overlap was determined using a potential which reproduced the results obtained from Green's function Monte Carlo calculations [16]. The $<^{16}\mathrm{C}|^{15}\mathrm{C}>$ overlap was built with a bound neutron wave function using a Wood-Saxon potential with r_0 = 1.25 fm and a = 0.65 fm using a proper depth to reproduce the neutron separation energy.

From the shape of angular distributions the angular momentum of the removed nucleon is deduced, finding consistent results with the previously known assignments for the bound states and the first resonance. In the case of the second resonance both l=1 and l=2 calculations are compared to the data. From the fit, l=2 is more favourable. However, the spectroscopic factor obtained from the fit allows to reject the l=2 since it yields nonphysical occupancy that would exceed the maximum single-particle strength available in the $0d_{5/2}$ orbital. Therefore, an assignment of l=1 was determined for this state. The state can be considered as a hole in the $0p_{3/2}$ orbital since the first resonance almost exhausts the occupation of the $0p_{1/2}$. Previous experiments have already determined the presence of an ℓ=1 state at an energy compatible with our

[1]The impact of the E_x in the single particle cross-section of the second resonance (the only state that we cannot firmly assign to any previous measurement) is orders of magnitude smaller than the quoted uncertainty.

Table 1. Fit results and relative spectroscopic factors compared to theoretical YSOX calculations. The quoted uncertainties are just statistical, the discussion of the systematic ones is included on the text.

E_x (MeV) (t,p) [5]	E_x (MeV)	l	J^π	C^2S	$E_{x,th}$	C^2S_{th}
	(d,t) [This work]				YSOX [3]	
0	-0.30(20)	0	$1/2^+$	0.65(16)	0	0.73
0.744	1.10(25)	2	$5/2^+$	1.35(32)	0.78	1.13
3.105	2.76(7)	1	$1/2^-$	1.74(23)	2.63	1.74
(5.866)	5.41(11)	1	$3/2^-$	1.25(24)	4.97	0.37
		1	$3/2^-$		6.10	0.93

energy measurement, considering the uncertainties, but they assigned it as a $1/2^-$ [5], not being able to exclude $3/2^-$.

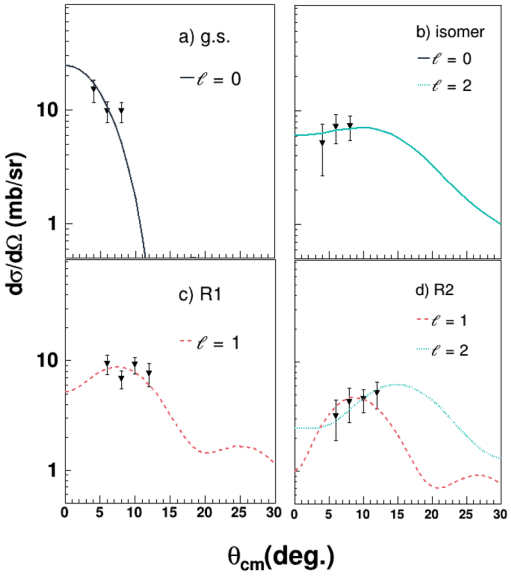

Figure 3. Angular distributions from the different states present in our data. Together with the experimental distributions DWBA calculations are normalized to the data. The shape from the distributions is used to determine the l number, finding consistent results between our data and the previous assignments (a-c). In the case of the second resonance we cannot firmly assign its l value by the shape, since both l=1 and 2 are compatible with our data.

Table 1 contains the compiled results of the fit compared with the states they are assigned and the relative spectroscopic factors which are obtained requiring that the sum of the $1/2^+$ and $5/2^+$ states is equal to 2, which assumes no occupancy of the $0d_{3/2}$. The table also presents the results of shell-model calculations performed with the YSOX interaction [3] which has proven to work well in the CNO neutron-rich region of the nuclear chart.

3.2 Discussion

The results of the spectroscopy of ^{15}C through the (d,t) reaction are presented in table 1. they show valence neutron configurations for the bound states which are in good agreement with previous measurements which used other probes such as knockout [8] and breakup reactions [7]. The C^2S values are also well reproduced by the YSOX interaction.

Above the one-neutron separation threshold the two states assigned l=1 are understood as 2p-1h configurations where two neutrons lay in the sd shell and the hole comes from the $0p_{1/2}$ and the $0p_{3/2}$ orbitals respectively. The spectroscopic factor of the first resonance, which carries most of the single particle strength of the $0p_{1/2}$ orbital, is in very good agreement with the C^2S value predicted by the shell model with the YSOX interaction.

For the second resonance the shell model calculations predict that the strength of the $0p_{3/2}$ orbital is spread over different states, but its two main fragments fall around the position of our resonance. As we observe experimentally the observed width of the second unbound state is compatible with the existence of two states together, an argument that supports that the contributions of the main fragments are being summed in a single state. Theoretical predictions of the shell-model with the YSOX interaction also support this argument since the sum of the C^2S of the two main states of the $0p_{3/2}$ orbital is in good agreement with our experimental result.

References

[1] T. Suzuki, R. Fujimoto and T. Otsuka, Phys. Rev. C 67 (2003) 044302.
[2] T. Suzuki and T. Otsuka, Phys. Rev. C 78 (2008) 061301(R).
[3] C. Yuan et al., Phys. Rev. C 85 (2012) 064324.
[4] J. Goss, Phys. Rev. C 8 (1973) 514-517.
[5] S. Truong, Phys. Rev. C 28 (1983) 977-979.
[6] F. Cappuzzello et al., Phys. Lett. B 711 (2012) 347.
[7] T. Yamaguchi et al., Nuc. Phys. A 724 (2003) 3.
[8] V. Maddalena et al., Phys. Rev. C 63 (2001) 024613.
[9] N. I. Ashwood et al., Phys. Rev. C 70 (2004) 024608.
[10] E. Pollacco et al., Eur. Phys. J. A 25 (2005) 287.
[11] A. Matta et al, J.Phys.G 43 (2016) 4, 045113.
[12] Haixia An et al, Phys. Rev. C 73 (2006) 054605.
[13] X.Pereira-Lopez, PhD Thesis (2016).
[14] X. Pereira-López, Phys. Lett. B 811 (2020) 135939.
[15] D.Y. Pang et al., Phys. Rev. C 79 (2009) 024615.
[16] I. Brida, S.C. Pieper, and R.B. Wiringa, Phys. Rev. C 84 (2011) 024319.